DOI: 10.1002/ejic.200500614

The Mechanism of Magnetic Interaction in Spin-Ladder Molecular Magnets: A First-Principles, Bottom-Up, Theoretical Study of the Magnetism in the Two-Legged Spin-Ladder Bis(2-amino-5-nitropyridinium) Tetrabromocuprate Monohydrate

Mercè Deumal,*[a] Giacomo Giorgi,[b] Michael A. Robb,[c] Mark M. Turnbull,[d] Christopher P. Landee,[e] and Juan J. Novoa*[a][‡]

Keywords: Copper / Density functional calculations / Magnetic properties / Spin-ladders / Structure-activity relationships

The magnetic properties of the isotropic ($J_{rail} \approx J_{rung}$), two-legged spin-ladder bis(2-amino-5-nitropyridinium) tetrabromocuprate monohydrate, $[(5NAP)_2CuBr_4 \cdot H_2O]$, have been studied using a first-principles, bottom-up approach, which allows computation of macroscopic magnetic properties (for instance, the magnetic susceptibility) of a crystal from only a knowledge of its crystal packing. Evaluation of the J_{AB} parameters, using the 163 K X-ray structure of $[(5NAP)_2CuBr_4 \cdot H_2O]$, indicates that the magnetic topology of this crystal is a two-legged antiferromagnetic spin-ladder, with values of J_{rail} and J_{rung} of $-22.2\ cm^{-1}$ and $-19.7\ cm^{-1}$, respectively. These values are very close to those that best fit the experimental magnetic susceptibility curve, which are $-13.59\ cm^{-1}$ and $-14.16\ cm^{-1}$, respectively. Very weak diagonal interactions within each ladder [$J(d3) = -0.9\ cm^{-1}$] and between nearby ladders [$J(d4) = -0.3\ cm^{-1}$] are also found. The computed magnetic susceptibility curve obtained using the two-legged spin-ladder properly reproduces the experimental magnetic curve (a quantitative agreement is obtained by applying a linear scaling factor of about 0.75 to the energies). The singlet–triplet spin-gap of this spin-ladder was computed to be 17 K, in close agreement with the experimental result (11 K). The change of the spin-gap/J_{rail} with the size (2xL) of the magnetic spin-ladder model space was found to converge towards 0.5, while that for a single-legged (1xL) spin-ladder converges towards zero, both in good agreement with the known trends for these systems.

Introduction

Current research in molecular magnetism (understood here as all forms of molecule-based magnetism) aims to rationally design and synthesize molecular materials with tailor-made magnetic properties that, in some cases, will coexist with other technological properties of interest, such as conductivity or superconductivity. As a result of the combined work of many experimental and theoretical groups, progress in the field during recent years has been spectacular.[1] A rational design of molecular magnets requires the existence of: (i) properly based magneto-structural correlations, which would allow us to correlate the nature of the magnetic interaction with the relative orientations of the radical units, (ii) a rigorous form for correlating the microscopic magnetic interactions with the macroscopic magnetic properties, (iii) a reliable methodology to predict the most likely polymorphs of a crystal, and (iv) methodologies to control the growth of the desired polymorph of a crystal. Progress along these lines has been achieved, however more is required before a rational design of molecular magnets can be achieved.

One form of improving our knowledge on magneto-structural correlations is by having a better (and properly based) knowledge of the mechanism of the magnetic interaction for materials that present properties of special interest. Such studies should be performed using a rigorous first-principles methodology that avoids approximations or over-simplifications and, thus, does not reach averaged results or misleading conclusions. These studies should allow us to generate a database of first-principles information regard-

[a] Departament de Química Física, Universitat de Barcelona and Centre de Recerca en Química Teòrica (CeRQT), Parc Científic de Barcelona,
Martí i Franquès 1, 08028 Barcelona, Spain
Fax: +34-93-402-1231
E-mail: m.deumal@qf.ub.es
juan.novoa@ub.edu
[b] Dipartimento di Chimica, Universita' degli Studi di Perugia, Via Elce di Sotto 8, 06123 Perugia, Italy
[c] Chemistry Department, Imperial College London, South Kensington Campus, London SW7 2AZ, UK
[d] Chemistry Department, Clark University, 950 Main St., Worcester, MA 01610, USA
[e] Physics Department, Clark University, 950 Main St., Worcester, MA 01610, USA
[‡] Associate Member of the CEPBA-IBM Research Institute
Supporting information for this article is available on the WWW under http://www.eurjic.org or from the author.

ing the keys governing the magnetic interaction in molecular materials.

Spin-ladders[2] are one of these materials of special interest. They result from assembling a given number (n) of chains (L) and connecting them magnetically (nxL). In the literature, the connected chains are referred to as either the legs or rails of the spin-ladder. The connections between the chains are referred to as rungs. Within this field, antiferromagnetic spin-ladders have attracted much interest for two main reasons: (i) their connection with high-temperature superconductors, which are lightly-doped 2D antiferromagnets, and (ii) the special properties that are present depending on the number of legs (ladders with an even number of legs present a finite spin-gap between singlet ground state, E_0, and lowest energy triplet state, E_1, energies, while ladders with an odd number of legs behave as single chains and show no spin-gap; such results have been verified both theoretically and experimentally[2]).

Up to now, the study of the magnetic properties of spin-ladders has been based on finding a good empirical model to fit the experimental magnetic susceptibility, and then rationalizing the experimental properties using the available solutions for that model, usually found in the literature as a function of the J_{rung}/J_{rail} ratio.[2] In this work we will carry out for the first time, to the best of our knowledge, a first-principles, bottom-up, theoretical analysis of the mechanism of magnetic interactions in a two-legged antiferromagnetic spin-ladder. We have selected for study the bis(2-amino-5-nitropyridinium) tetrabromocuprate monohydrate spin-ladder [see Figure 1 (a)], herein identified as [$(5NAP)_2CuBr_4{\cdot}H_2O$], whose crystal structure has been determined by X-ray diffraction at 163 K. This is an antiferromagnetic, two-legged spin-ladder[3] with the added interest of having similar values for the experimental J_{rail} and J_{rung} values (–13.59 and –14.16 cm^{-1}, respectively, obtained from fitting the magnetic susceptibility as a function of temperature). The isotropic exchange ($J_{rail} \approx J_{rung}$) case is where the effect of the quantum fluctuations is most pronounced; the physics is the most complex and cannot be properly treated by perturbation theory. We will apply to [$(5NAP)_2CuBr_4{\cdot}H_2O$] our recently proposed, first-principles, bottom-up, theoretical procedure[4] to find the mechanism of the magnetic interaction within this system and properly justify the available experimental magnetic data.

Our first-principles, bottom-up, theoretical analysis of molecular magnetic materials[4] is a tool that connects the microscopic and macroscopic magnetic properties using a rigorous numerical procedure. It could thus become a practical tool for the rational design of molecular magnets, once good magneto-structural correlations are found[5] and a better control of the crystal packing prediction and growth is also achieved. The first-principles, bottom-up, theoretical analysis starts by computing the strength of all unique radical–radical magnetic interactions (the J_{AB} constants of the Heisenberg Hamiltonian). There are no prior assumptions of the relative importance of J_{AB}, so the procedure is fully nonbiased. The values of the J_{AB} magnetic interactions are then used to define the magnetic topology of the crystal,[6]

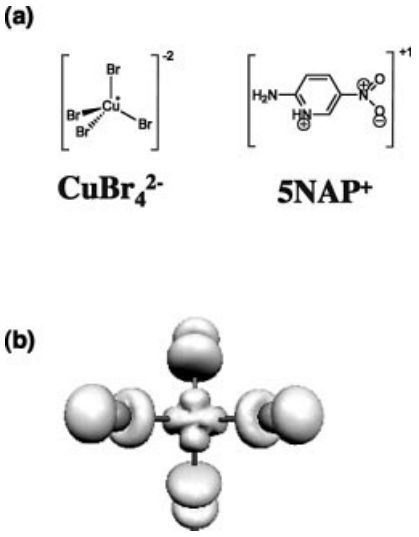

Figure 1. (a) Structure of the ions present in [$(5NAP)_2CuBr_4{\cdot}H_2O$]. (b) Spin distribution in the $CuBr_4^{2-}$ anion (isodensity surface of 0.002 au).

a property that allows the selection of a finite model space representative of the magnetic interactions in the full-sized crystal. The matrix representation of the Heisenberg Hamiltonian is then computed in the space of all the spin functions of the finite model space, and the energy of all possible magnetic states is calculated by diagonalization of that matrix. This allows the connection of the microscopic and macroscopic [e.g. magnetic susceptibility $\chi(T)$ and heat capacity $C_p(T)$] magnetic properties using the appropriate expressions from statistical mechanics.[4] The magnetic topology also allows identification of the magnetic pathways along which the magnetic interactions propagate over the whole crystal. We should mention that this first-principles, bottom-up, theoretical approach has already been successfully applied to the study of the magnetic properties of a variety of prototype systems.[4,7]

Results and Discussion

Here we will briefly describe the main steps and underlying physics behind the first principles, bottom-up procedure that we will then apply to the study of [$(5NAP)_2CuBr_4{\cdot}H_2O$]. For the interested reader, a detailed mathematical and physical account of the procedure and its basis is available in the literature.[4]

We have found that the following four steps allow us to carry out the proposed first principles, bottom-up procedure in a nonbiased form:

1) The first step consists of performing a detailed analysis of the crystal packing to identify all unique A-B radical–radical pairs whose interpair distance is smaller than a given threshold value (above which the magnetic interaction between radicals is expected to be negligible). This threshold is deliberately chosen to select more pairs than the first nearest neighbors (the usual candidates in the literature).

Such a selection procedure of radical–radical pairs is completely nonbiased.

2) Secondly, for all A-B radical–radical pairs selected in the previous step, we evaluate the value of the corresponding J_{AB} magnetic interactions using quantum chemical methods.

3) Using the computed J_{AB} parameter values, we then determine the magnetic topology of the crystal in terms of how non-negligible J_{AB} interactions propagate along the crystal axes. Two neighboring A-B radical sites are connected whenever its magnetic interaction presents a $|J_{AB}|$ value larger than a given threshold, which in previous calculations was estimated to be $|0.05|$ cm^{-1}. Then, we search for the smallest (finite-sized) minimal magnetic model space that describes the magnetic interactions of the whole crystal in a balanced way. The repetition of such a minimal model along the (*a*,*b*,*c*) crystallographic directions should regenerate the magnetic topology of the whole crystal. The radical centers constituting the minimal magnetic model define a spin-space that is used to compute the matrix representation of the corresponding Heisenberg Hamiltonian (see Computational Data section). Note that the only parameters required to compute that matrix representation of the Heisenberg Hamiltonian are the J_{AB} parameters computed in step 2.

4) In the fourth and final step, the Heisenberg Hamiltonian matrix is diagonalized to obtain the energy for all possible spin-states. These energies are then used to compute the magnetic susceptibility $\chi(T)$ and/or heat capacity $C_p(T)$ using the appropriate expressions obtained from a statistical mechanical treatment.[4]

The magnetic properties of $[X_2CuBr_4]$ compounds have been reported for a large variety of systems.[8] The packing of these crystals can be modified by changing the size and shape of the X^+ organic cation, which, in turn, induces modifications in the observed magnetic properties. Some of these $[X_2CuBr_4]$ crystals are low-dimensional 1D and 2D magnetic systems.

The structure of the $[(5NAP)_2CuBr_4{\cdot}H_2O]$ ionic crystal was determined by X-ray diffraction at 163 K.[3] It crystallizes in the $P\bar{1}$ space group, with cell parameters a = 7.566, b = 9.359, c = 14.909 Å, α = 77.073°, β = 75.912°, γ = 76.393°, and Z = 2. The packing can be rationalized as a stack of double-decked planes [see Figure 2 (a) for a general view and Figure 2 (b) for a view of a single double-decked plane]. Each individual plane constituting the double-decked planes [Figure 2 (c)] presents a structure where the $5NAP^+$ cations surround the $CuBr_4^{2-}$ anions in a T-shaped disposition (this allows the formation of short C–H···O contacts between the cations, with distances within the 2.46–2.56 Å range, in addition to the C–H···Br contacts between anions and cations, in the 3.0–3.2 Å range). The disposition of the spin-containing units (the $CuBr_4^{2-}$ anions) in the crystal is shown in Figure 3. The topology of a two-legged ladder along the crystal *a*-axis, previously proposed to explain the magnetism of this crystal,[3] is clearly observed when looking at the shortest intermolecular Cu···Cu distances [6.34 and 7.57 Å; Figure 3 (b)].

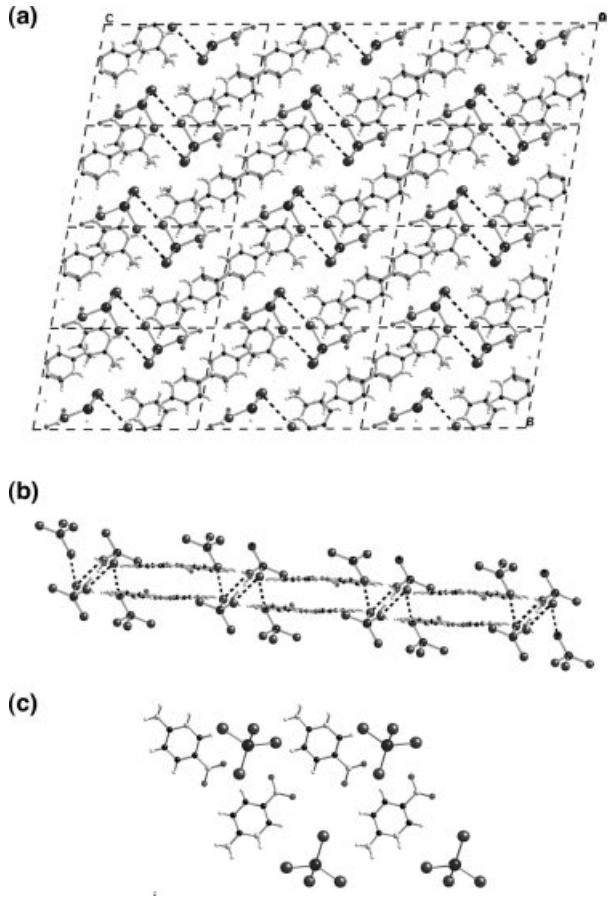

Figure 2. (a) *bc*-view of the $[(5NAP)_2CuBr_4{\cdot}H_2O]$ ionic crystal, where double-decked planes run along the *a*-axis (Br···Br contacts in the 3.9–4.1 Å range are indicated). (b) View along the *a*-axis of a double-decked plane. (c) *bc*-view of one of the two planes forming the double-decked planes, where the $5NAP^+$ cations surround the $CuBr_4^{2-}$ anions in a T-shaped disposition.

The only available experimental data on the magnetic properties of this crystal are magnetic susceptibility measurements.[3] The experimental $\chi(T)$ data were fitted to a two-legged spin-ladder model based on two facts: (i) the magnetic pathways between $CuBr_4^{2-}$ radicals were expected to be through-space (by means of short Br···Br contacts), and (ii) the shortest Cu···Cu (and Br···Br) contacts showed the topology of a two-legged spin-ladder [see Figure 3 (b)]. The expression used for fitting the experimental $\chi(T)$ data for the spin-ladder was derived by extensive Monte Carlo calculations using a Heisenberg Hamiltonian that included both J_{rung} and J_{rail} at an arbitrary ratio of the two interactions.[3c] Johnston et al.[3c] have obtained two different expressions for the spin-ladder susceptibility, depending on the ratio J_{rung}/J_{rail}. Both expressions were applied to fit the experimental data without knowing in advance the ratio of the exchange parameters. The dominant rung expression ($|J_{rung}| > |J_{rail}|$) gave an excellent description of our data with the reported J_{rung} = –14.16 cm^{-1} and J_{rail} = –13.59 cm^{-1};[3a] the dominant rail expression ($|J_{rung}| < |J_{rail}|$) would not converge, yielding a susceptibility curve of entirely the wrong shape, for any combination of parameters.

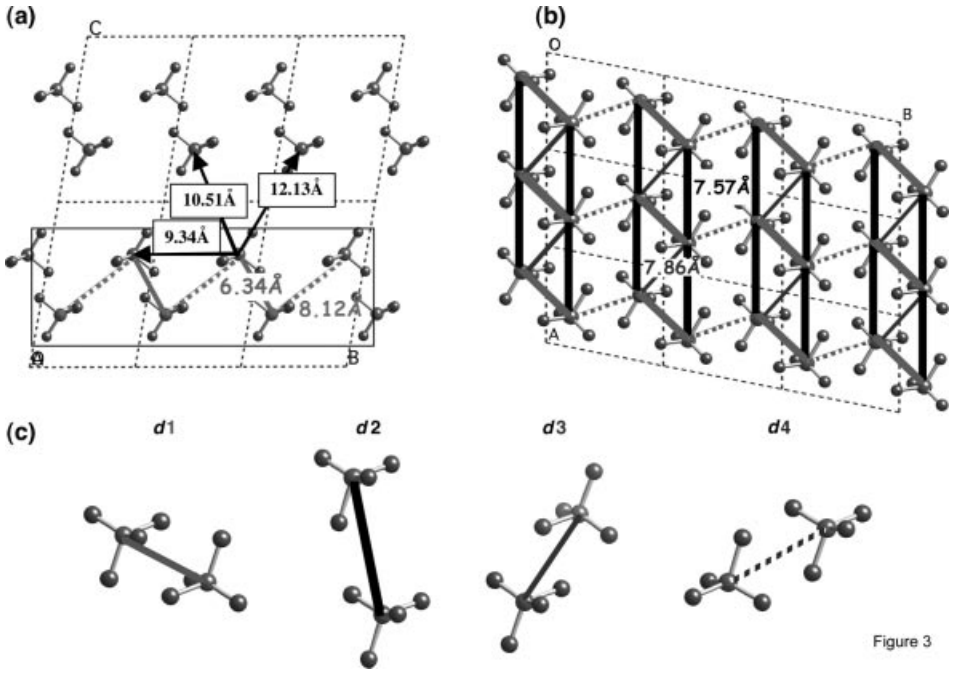

Figure 3. Views of the $CuBr_4^{2-}$ anion within the structure of the $[(5NAP)_2CuBr_4{\cdot}H_2O]$ crystal along (a) the *bc* and (b) the *ab* crystallographic axes. Note that the Cu···Cu distances for all *di* radical pairs are given. The topology of a two-legged ladder is clearly envisaged. (c) Selected *di* radical pairs verifying a spin-carrier interradical distance cutoff of 8.5 Å (see Table 1 for details on main distances).

At this point, it is essential to stress that, although a ladder model was explicitly used to fit the experimental available $\chi(T)$ data by means of J_{rung} and J_{rail}, it could not get the origin of these *J*'s. As we will show shortly, we can contribute to explicitly get the origin of J_{rung} and J_{rail} by identifying the radical pairs that are responsible for such microscopic magnetic interactions.

Keeping in mind the packing described above for the $[(5NAP)_2CuBr_4{\cdot}H_2O]$ crystal, we can now start the first-principles, bottom-up study of the magnetism of this crystal. On the basis of calculations that show that the $CuBr_4^{2-}{\cdots}CuBr_4^{2-}$ magnetic interaction becomes negligible at Cu···Cu distances above 8.5 Å, in step (1) we selected all $CuBr_4^{2-}{\cdots}CuBr_4^{2-}$ pairs with Cu···Cu distances shorter than 8.5 Å [see Figure 3 (a) and (b)]. This resulted in the four $CuBr_4^{2-}{\cdots}CuBr_4^{2-}$ pairs depicted in Figure 3 (c) whose Cu···Cu distances are 6.34, 7.57, 7.86, and 8.12 Å [the next three pairs of radicals have Cu···Cu pair distances of 9.34, 10.51, and 12.13 Å, see Figure 3 (a)]. Each radical–radical pair is identified as *d*1–*d*4, according to an increasing ordering of the Cu···Cu distance (Table 1 contains the values of the main intermolecular parameters).

We can now proceed to step (2) and compute the value of J_{AB} for all *di* radical–radical pairs selected in step (1). As mentioned above, these parameters are obtained by subtracting the total energy of the singlet and triplet states for each *di* radical–radical pair at its crystal geometry. One could think of doing such a calculation using an $(anion)_2$ cluster, but numerical tests (see Table 1 and discussion below) indicated that the $(anion)_2$ cluster does not properly reproduce the electronic structure of the radical anions within the crystal and that one has to include in the calculation at least the first-neighboring cations of the radical-anion pairs of interest. Therefore, the calculation must be done on an $(anion)_2(cation)_x$ cluster. As the crystal is neutral, we selected four cations to build a neutral $(anion)_2(cation)_4$ cluster (note that, in this case, the anions have a –2 charge and the cations have +1 charge). The inclusion of the cations also has an extra advantage as it automatically takes into account the possible participation of the diamagnetic cations in the through-space radical–radical magnetic interaction.

Table 1. Values of the Cu···Cu and shortest Br···Br distances for the four $CuBr_4^{2-}{\cdots}CuBr_4^{2-}$ radical–radical pairs of the $[(5NAP)_2CuBr_4{\cdot}H_2O]$ crystal having a Cu···Cu distance smaller than 8.5 Å [see Supporting Information Figure S1 for the actual geometry of the *d*1–*d*4 $(anion)_2(cation)_4$ clusters used to compute *J*(*di*)]. Also included are the values of the *J*(*di*) parameters for each pair.

di	Cu···Cu [Å]	Br···Br [Å]	Model	*J*(*di*) [cm^{-1}]
*d*1	6.34	4.07(2) – 4.25 – 5.98(2)	$(anion)_2$	–43.54
			$(anion)_2(cation)_4$	–19.73
*d*2	7.57	3.93 – 6.00 – 6.32	$(anion)_2$	–28.38
			$(anion)_2(cation)_4$	–22.17
*d*3	7.86	4.68 – 4.94(2) – 7.26	$(anion)_2$	+0.18
			$(anion)_2(cation)_4$	–0.85
*d*4	8.12	5.24(2) – 6.13 – 6.62	$(anion)_2$	–0.79
			$(anion)_2(cation)_4$	–0.31

There is more than one form of selecting four cations for each di radical–radical pair [see Figure 3 (c) for *d*1–*d*4]. Therefore, we have to evaluate the effect that such selection has on the computed J_{AB} values [hereafter *J*(*di*)]. We did this evaluation for all four pairs, but we only report the results for *d*1, as the trends are similar in all cases. The test was done using the three $(anion)_2(cation)_4$ clusters shown in

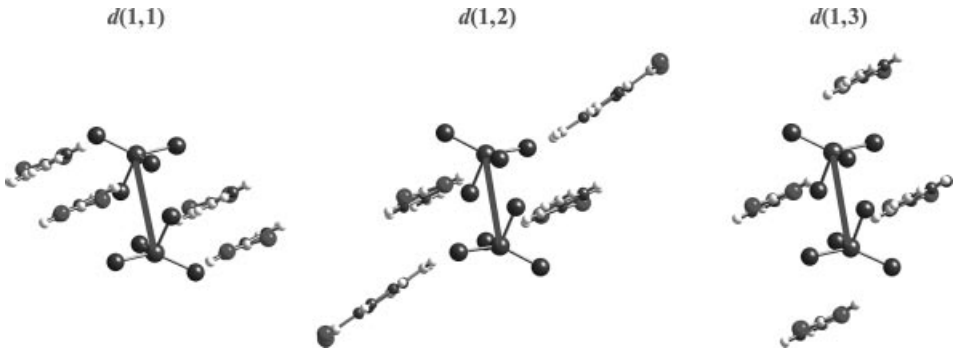

Figure 4. Geometry of the various $(anion)_2(cation)_4$ clusters used to evaluate the effect of the selected cations on the computed $J(d1)$ value.

Figure 4, identified as $d(1,1)$, $d(1,2)$, and $d(1,3)$. The results collected in Table 2 show a change smaller than 3 cm^{-1} in the computed $J(d1)$ value. We also tested the effect that the Madelung field[9] generated by the rest of the crystal has on the computed $J(d1)$ value. For the specific case of the $d(1,2)$ cluster (see Figure 4), the computed $J(d1)$ value accounting for the Madelung field is –19.84 cm^{-1}, while without this field it is –19.73 cm^{-1}. Due to the small impact of the inclusion of the Madelung field, we did not evaluate its effect on the other di radical–radical pairs. Finally, we can discuss the origin of the difference between the $J(d1)$ results obtained using either an $(anion)_2(cation)_4$ model [e.g. the $d(1,2)$ cluster] or an only an $(anion)_2$ cluster (J_{AB} values of –19.73 and –43.54 cm^{-1}, respectively). To test if this difference is due to the lack of electrostatic confinement induced by the cations in the anion wavefunction, we did further calculations to mimic such electrostatic effects by using point atomic charges (fitted to reproduce the electrostatic potential of the nuclei of the isolated cations) instead of the atoms themselves. The computed J_{AB} value was –26.60 cm^{-1}, which differs by 6.87 cm^{-1}, in absolute terms, from the computed J_{AB} using the $d(1,2)$ $(anion)_2(cation)_4$ cluster. Such small difference can be attributed to two factors: (a) the use of point charges does not reproduce the Pauli repulsion (due to the Pauli Exclusion Principle) induced by the electrons of the cations on the electrons of the anions, and (b) the presence of a cation-mediated through-space interaction, where the cation orbitals are used to magnetically connect the anions (a sort of superexchange through-space mechanism). It is difficult to evaluate the relative importance of each factor accurately, but in any case our results indicate that it is safer to use $(anion)_2(cation)_4$ clusters to include both a proper description of the anions' environment and any possible cation-mediated exchange.

Table 2. Dependence of the computed $J(d1)$ value on the selected cations included in the $(anion)_2(cation)_4$ cluster. The values are for the $d(1,1)$, $d(1,2)$, and $d(1,3)$ $(anion)_2(cation)_4$ clusters shown in Figure 4.

d(1,*j*)	$J(d1,j)$ [cm^{-1}]	Model
$d(1,1)$	–19.05	$(anion)_2(cation)_4$
$d(1,2)$	–19.73	$(anion)_2(cation)_4$
	–19.84	$(anion)_2cation_4$ + Madelung (ref.[16])
$d(1,3)$	–16.18	$(anion)_2(cation)_4$

Table 1 shows the all computed $J(di)$ values using appropriate $(anion)_2(cation)_4$ clusters. All four $J(di)$ magnetic interactions are antiferromagnetic, with $J(d1)$ and $J(d2)$ almost identical and much larger than the values of $J(d3)$ and $J(d4)$. These results show that there is no direct correspondence between the Cu···Cu and Br···Br distances and the size of the $J(di)$ parameter. The value and connectivity of the $J(di)$ magnetic interactions define the magnetic topology of the $[(5NAP)_2CuBr_4{\cdot}H_2O]$ crystal (see Figure 5). The main magnetic motif consists of two-legged spin-ladders along the crystallographic *a*-axis, where $J_{rail} = J(d2) =$ –22.17 cm^{-1} and $J_{rung} = J(d1) =$ –19.73 cm^{-1}. Within any individual two-legged spin-ladder there is a small diagonal magnetic interaction, $J(d3) =$ –0.85 cm^{-1}, and adjacent two-legged spin-ladders interact very weakly along the *b*-axis through $J(d4) =$ –0.31 cm^{-1}. Therefore, the magnetic topology of $[(5NAP)_2CuBr_4{\cdot}H_2O]$ seems to be better described as consisting of isolated two-legged spin-ladders (a 1D topology), but could also be described as a set of noninteracting *ab*-planes, each formed by weakly interacting, two-legged spin-ladder motifs (a 2D topology). Below, we will show the results of numerical simulations that indicate that the 1D topology gives a proper description of the magnetism for $[(5NAP)_2CuBr_4{\cdot}H_2O]$.

To perform steps (3) and (4) of the bottom-up procedure, we have to select a minimal magnetic model space. For an isolated two-legged spin-ladder, based on previous work,[7] we expect that a four-sites (4s) model [Figure 6 (a)] should be an appropriate minimal magnetic model space. For $[(5NAP)_2CuBr_4{\cdot}H_2O]$, we will validate this model by studying the convergence of the macroscopic magnetic susceptibility $\chi(T)$ values when the minimal 4s model is replicated along the three crystallographic axes. Thus, the 4s model is propagated along (i) the *a*-axis, obtaining the 6s, 8s, ..., up to 14s models [Figure 6 (a)], and (ii) the *b*-axis by selecting the 4s4s and 4s4s4s models [Figure 6 (b)]. No replication is required along the *c*-axis, as there are no J_{AB} magnetic interactions along this direction, therefore the propagated model gives exactly the same results as the 4s model. As a further test, we also propagated the 4s4s model along the *a*-axis to generate the 6s6s and 8s8s models. The matrix

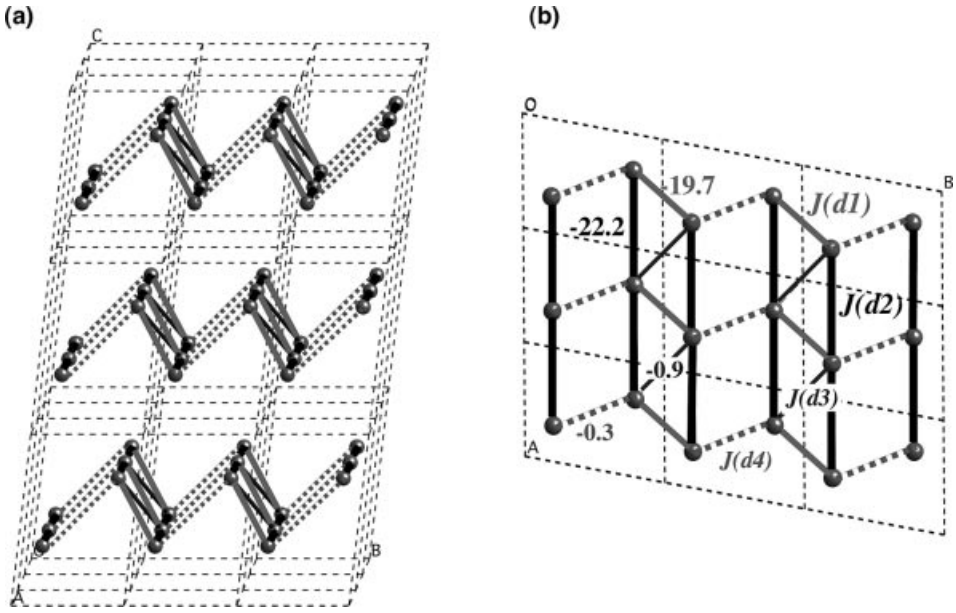

Figure 5. Magnetic topology of the $[(5NAP)_2CuBr_4{\cdot}H_2O]$ crystal: (a) magnetically noninteracting *ab*-layers; (b) magnification of any given *ab*-layer, which consists of two-legged spin-ladder motifs with $J(d2) = -22.2\ cm^{-1}$ as rail and $J(d1) = -19.7\ cm^{-1}$ as rung magnetic interactions. Within any individual two-legged spin-ladder there is a small diagonal magnetic interaction, $J(d3) = -0.9\ cm^{-1}$, and adjacent two-legged spin-ladders interact very weakly along the *b*-axis through $J(d4) = -0.3\ cm^{-1}$.

representation of the Heisenberg Hamiltonian was built[11] and diagonalized for all these model spaces. The resulting energy levels and corresponding spin quantum numbers were then used to calculate the magnetic susceptibility $\chi(T)$ (see Figure 6).

The simulated $\chi(T)$ data shown in Figure 6 allow us to conclude: (i) all the $\chi(T)$ curves show a shape similar to the experimental curve; (ii) there is a good convergence on $\chi(T)$ as the size of the model increases by propagating the minimal 4s model along both the *a*-axis [Figure 6 (a)], and the

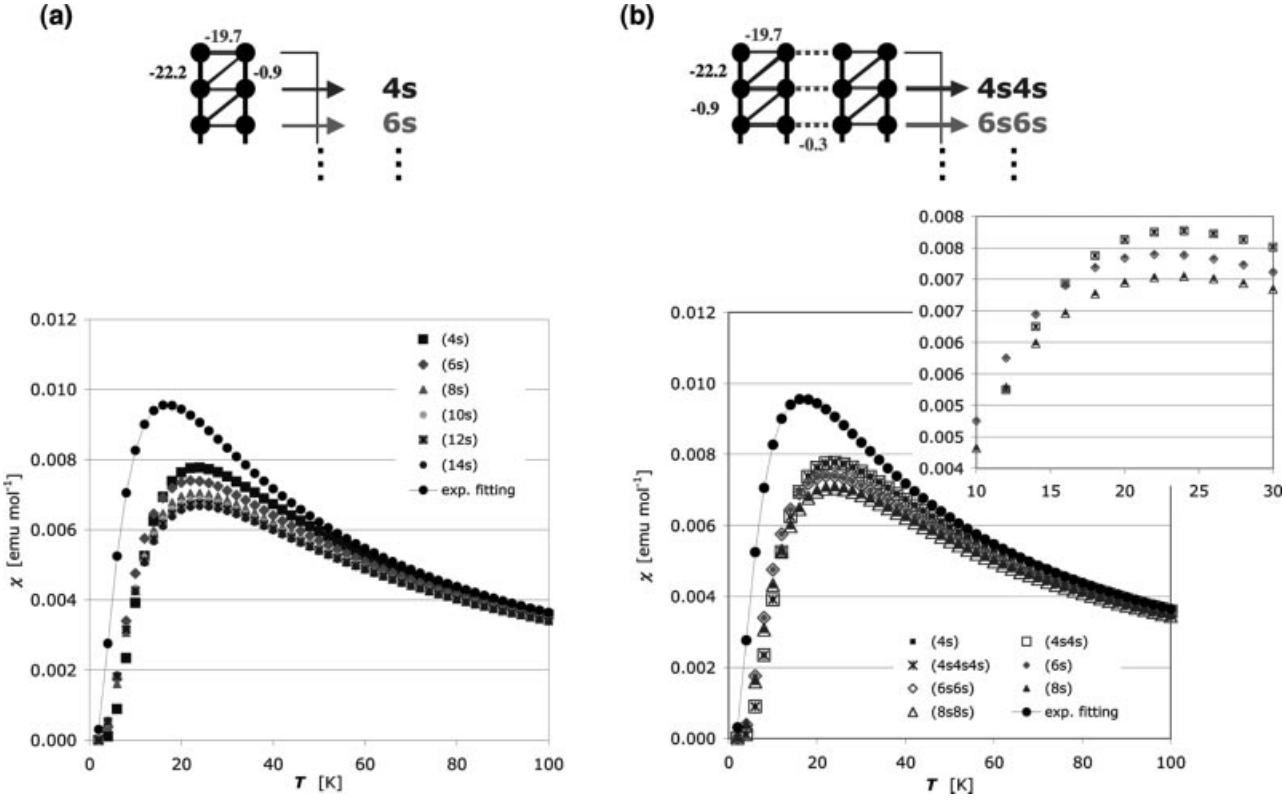

Figure 6. Magnetic susceptibility $\chi(T)$ numerically calculated values extending the minimal 4s magnetic model along the (a) *a*-axis (intra spin-ladder 6s–14s models) and (b) *b*-axis (inter spin-ladder 4s4s, 4s4s4s, 6s6s and 8s8s models).

b-axis [Figure 6 (b)]; and (iii) the $\chi(T)$ values obtained with the inter-ladder *nsn*s models reproduce the $\chi(T)$ values obtained using the intra-ladder *ns* models perfectly [Figure 6 (b)], thus suggesting that there is no need to account for $J(d4)$ in the minimal magnetic model space. The latter conclusion is the final indication that our magnetic topology consists of basically noninteracting spin-ladders, i.e. it is a 1D topology.

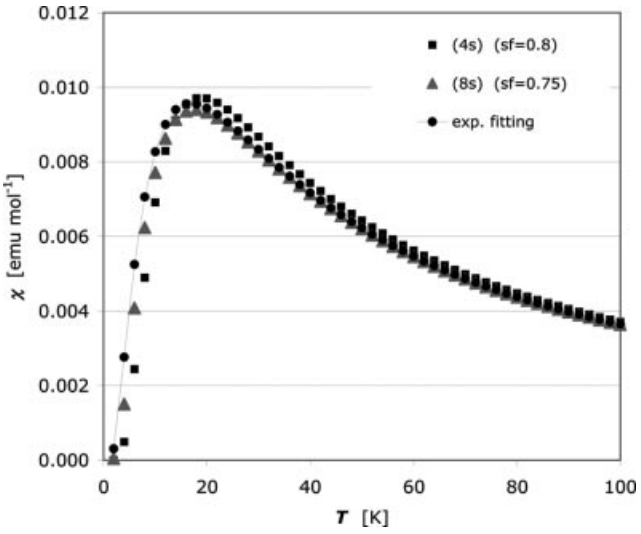

Figure 7. Required scaling factor (sf) to quantitatively reproduce the experimental magnetic susceptibility $\chi(T)$ data using both a 4s and an 8s model.

Although in all cases the shape of the computed magnetic susceptibility curves closely resembles the experimental curve, the agreement is not perfect. Previous studies[7] have suggested that such a difference can be attributed to various factors: (i) the use of high-temperature crystal structures, (ii) errors due to the use of a nonexact DFT functional and the broken-symmetry approach, and (iii) the use of a cluster approximation to compute the values of the $J(di)$ parameters, which neglects possible collective effects. In the case of $[(5NAP)_2CuBr_4{\cdot}H_2O]$, the crystal structure used throughout this study was determined at 163 K, which is a low enough temperature as to expect only small distortions due to temperature factors. We have also found[7] that it is possible to account for the difference between computed and experimental magnetic susceptibility curves by applying a constant linear scaling factor to all energy levels. For $[(5NAP)_2CuBr_4{\cdot}H_2O]$, when we apply a factor of 0.8 to all energy levels of the 4s minimal model we can quantitatively reproduce the experimental $\chi(T)$ curve (Figure 7). However, an even better agreement is found by applying a linear scaling factor of 0.75 to the 8s model (Figure 7).

A final test of the quality of the first-principles, bottom-up procedure in describing the properties of two-legged spin-ladder systems consists of computing the value of the singlet–triplet spin-gap (experimental data[3,12] indicate that

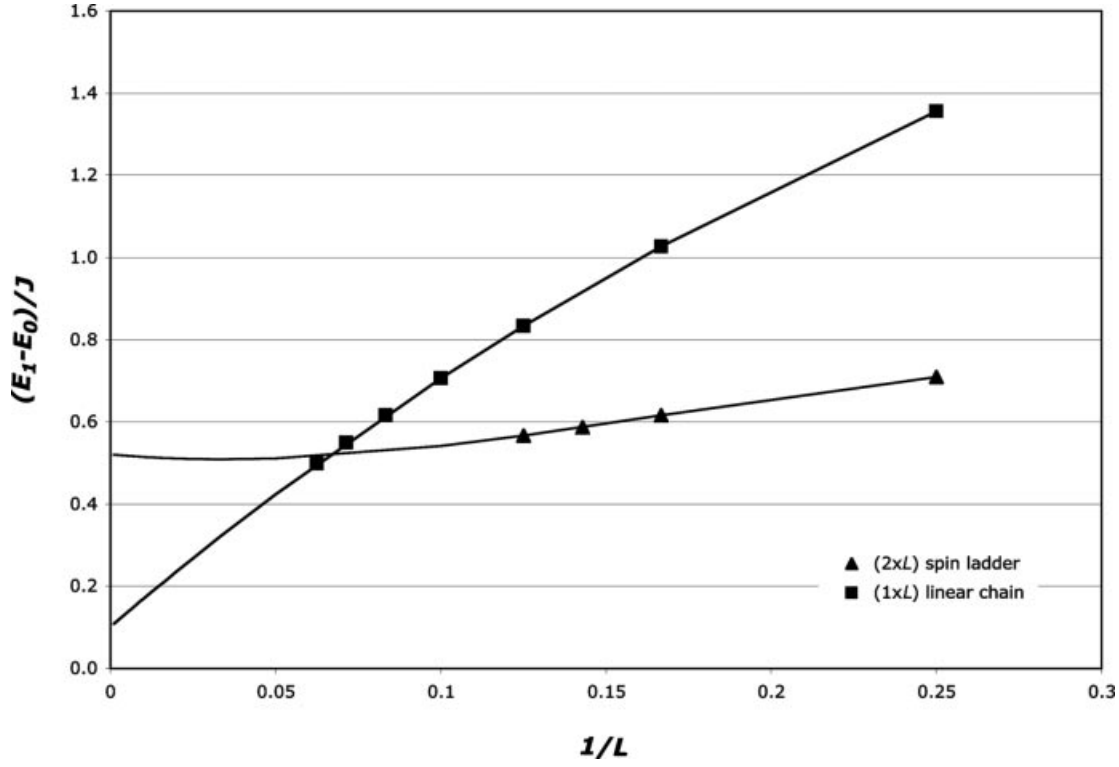

Figure 8. Values of $\Delta = (E_1 - E_0)/J$ as a function of the length of both a two-legged (2xL, with L = 4–8) and a single-legged (1xL, with L = 4–16) spin-ladder. In both cases the Δ values vary as $1/L$. In the limiting case of an infinite, two-legged spin-ladder the extrapolated Δ value is 0.5211. For an antiferromagnetic single-legged spin-ladder (i.e. a linear chain), the extrapolated result of Δ for the infinite chain (i.e. $1/L = 0$) is 0.1015, which is slightly larger than the expected zero value.

it should be 11 K) and its changes with the size of the model space. For a two-legged spin-ladder, previous studies indicate that there is a finite spin-gap[2] whose value decreases as the size of the model space increases.[2] Using the 4s magnetic model space with a linear scaling factor of 0.8, the computed value of the singlet–triplet spin gap ($E_1 - E_0$) is 24.24 K, about twice the experimental value. However, it decreases to 17.0 K when using the 8s model with a linear scaling factor of 0.75. Furthermore, as shown in Figure 8, the value of the expression $\Delta = (E_1 - E_0)/J$ decreases with the ladder length (2xL, with L = 4–8) as 1/L, as reported in the literature.[2] Extrapolating our fitted results to an infinite two-legged spin-ladder we found a Δ value of 0.5211 (see Figure 8), which agrees well with the best estimates (0.504) of this property.[2] As a further test, we also computed the value of $\Delta = (E_1 - E_0)/J$ for an antiferromagnetic single-legged spin-ladder (that is, a linear chain) for lengths L = 4–16. For an infinite linear chain, Δ is expected to be zero.[2] The results, also shown in Figure 8, follow a similar trend with respect to 1/L to those reported in the literature:[2] as L increases, the value of Δ approaches zero. However, our extrapolated result of Δ for the infinite chain (i.e., 1/L = 0) is 0.1015, which is slightly larger than zero. This small deviation is due to the fact that it may be necessary to look at a chain as long as 100 spins to actually see the gap vanish,[2] and this is obviously out of the reach of our current code. However, we have successfully described the main trends known for the spin-gap of the two main classes of spin-ladders. Consequently, we can conclude that our first-principles, bottom-up procedure properly describes the experimentally known properties of spin-ladder magnets.

Conclusions

Using the X-ray crystal structure determined at 163 K, we have computed the magnetic interactions in the [$(5NAP)_2CuBr_4 \cdot H_2O$] crystal. There are two dominant antiferromagnetic interactions, whose magnetic topology is found to consist of noninteracting, two-legged spin-ladders, with similar values for the rail $J(d2)$ (–22.2 cm^{-1}) and rung $J(d1)$ (–19.7 cm^{-1}) magnetic interactions. It is essential to stress that our contribution has been to explicitly get the origin of J_{rung} and J_{rail} by identifying the $(anion)_2(cation)_4$ clusters that are responsible for such microscopic magnetic interactions. The magnetic topology is in agreement with the experimentally proposed magnetic pathways, which were based only on the crystal packing of the $CuBr_4^{2-}$ radical-anions within the [$(5NAP)_2CuBr_4 \cdot H_2O$] crystal. However, we believe that the exchange interaction between Cu^{2+} ions does not only result from Br···Br direct contacts, but also from $5NAP^+ \cdots CuBr_4^{2-}$ contacts, since the organic ligands play the role of spin couplers.

The simulated $\chi(T)$ data reproduce the shape of the experimental $\chi(T)$ curve, although a linear scaling factor of about 0.75 is required to quantitatively reproduce the experimental values. Such a factor compensates for the use of a high-temperature (163 K) X-ray crystal structure and errors associated with the quantum chemical methods employed to compute the $J(di)$ parameters.

We have computed the singlet–triplet spin-gap ($E_1 - E_0$) for [$(5NAP)_2CuBr_4 \cdot H_2O$] two-legged spin-ladder and found it to be in the range of the experimental results (11 K). Furthermore, the values of $\Delta = (E_1 - E_0)/J$ show the same dependence on 1/L (L being the length of the spin-ladder) as reported in the literature: for a two-legged spin-ladder Δ decreases towards 0.5211 as 1/L tends to zero, while for a single-legged spin-ladder Δ approaches a value near zero (we believe that the small differences with the tabulated results[2] are due to the fact that it may be necessary to look at a chain as long as 100 spins to actually see the gap vanish, which is out of the reach of our current code).

Computational Data

The basic idea behind our first principles, bottom-up procedure[4] is to find a finite model space that properly describes the properties of the magnetic topology of the crystal. Within this space we then compute the matrix representation of the Heisenberg Hamiltonian (1)

$$\hat{H} = -\sum_{A,B}^{N} J_{AB}(2\hat{S}_A \cdot \hat{S}_B + \tfrac{1}{2}\hat{I}_{AB}) \quad (1)$$

where $\hat{S}_A$ is the spin operator associated with radical A, and $\hat{I}_{AB}$ the identity operator. Note that the only variables in this Hamiltonian are the microscopic J_{AB} parameters, which define the nature and size of the radical–radical magnetic interactions present in our model space. These microscopic J_{AB} parameters depend on the relative orientation of the radicals A and B, and can be computed using the appropriate quantum chemical methods. Once the matrix representation of the Heisenberg Hamiltonian is known, we can compute the energy spectrum of all spin states, and then apply the corresponding statistical mechanics expressions to compute the macroscopic magnetic properties of interest [$\chi(T)$, $C_p(T)$, ...]. Note that the individual energy values obtained by diagonalizing expression (1) are equivalent to those obtained using the more familiar $\hat{H} = -2\Sigma J_{AB}\hat{S}_A \cdot \hat{S}_B$ Heisenberg Hamiltonian, except for a shift in all energy values. Therefore, the corresponding energy differences will be the same. As the statistical mechanics expressions used to compute $\chi(T)$ and $C_p(T)$ use energy differences, both Hamiltonians give the same macroscopic results.

The entire procedure depends only on the microscopic radical–radical magnetic interactions (J_{AB}). The values of the J_{AB} parameters are also used to define the magnetic topology in terms of the connectivity that the J_{AB} parameters establish between the radicals that form the crystal. The magnetic topology provides a very useful pictorial representation of the magnetism within the crystal.

The minimal magnetic model space must be small enough to keep the Heisenberg Hamiltonian matrix at a reasonable size (in our current implementation $N \leq 16$ spin radical sites), but it must also be large enough to contain all significant magnetic pathways detected within the crystal. From our experience, the most important step in the above procedure is the selection of a proper minimal magnetic model space. In order to legitimate the selected minimal magnetic model space, we check the convergence of macroscopic properties [e.g. $\chi(T)$] as the model space is replicated along the three crystallographic directions by applying a regionally reduced density matrix approach: if the minimal magnetic model space is properly

chosen, the computed $\chi(T)$ values using such extended models should rapidly converge to the values obtained with the non-replicated minimal model space. All sets of results should also numerically reproduce the experimental $\chi(T)$ data.

As indicated above, the values of the microscopic J_{AB} pair interactions are computed using quantum chemical methods. In the $[(5NAP)_2CuBr_4{\cdot}H_2O]$ crystal, the $CuBr_4^{2-}$ anions are the only spin-carrier units; the $5NAP^+$ cations are closed-shell molecules with no spin whose primary function in the crystal is to act as spacers of the $CuBr_4^{2-}$ spin-carrier units. The ground electronic state of $CuBr_4^{2-}$ anions is a doublet, with the spin partially distributed over the bromine and Cu^{II} atoms (Figure 1, b). As the radicals are doublets, the value of J_{AB} is obtained by subtracting the energy of the most stable open-shell singlet (E^S_{BS}) and triplet (E^T) states, both computed at the geometry of the radical–radical pair found in the crystal, according to Equation (2).

$$J_{AB} = E^S_{BS} - E^T \quad (2)$$

The broken-symmetry approximation[13,14] is used to compute the energy of the open-shell singlet state. The E^S_{BS} and E^T energy values have been computed using the UB3LYP functional[15] (a 10^{-8} convergence criterion on the total energy and 10^{-10} on the integrals was used to ensure enough accuracy in the computation of the J_{AB} parameters). All DFT calculations performed in this study were carried out using the Gaussian-03 package.[16] We used in our calculations an Ahlrichs all-electron basis set[17] for Cu, and a 6-31+G basis set[18] for C, H, N, and O. For Br^-, we used the 6-31+G(d) basis set.[19]

Supporting Information: Table S1 shows the charges computed according to a Merz–Singht–Kollman scheme and employed to account for the Madelung field created by the nearest-neighboring $CuBr_4^{2-}$ anions and $5NAP^+$ cations to the *d*(1,*2*) $(anion)_2(cation)_4$ cluster. Figure S1 shows the final geometry of *d*1–*d4* of the $(anion)_2(cation)_4$ clusters used to compute *J*(*di*).

Acknowledgments

M. D. and J. J. N. acknowledge the Spanish "Ministerio de Ciencia y Tecnología" (BQU2002-04587-C02-02), and the Catalan "CIRIT" (2001SGR-0044) for funding. The authors also thank the CEPBA-IBM Research Institute, CEPBA and CESCA for allocation of CPU time on their computers. M. D. acknowledges the financial support of the "Ramón y Cajal" Program of the Spanish "Ministerio de Educación y Ciencia". G. G. acknowledges the European Union for funding within the "Transnational Access of HPC-Europe" Program (RII3-CT-2003-506079). M. M. T. and C. P. L. acknowledge financial support from the NSF (USA) grant DMR-9803813.

[1] a) *Magnetic Molecular Materials* (Eds.: D. Gatteschi, O. Kahn, J. S. Miller, F. Palacio), NATO ASI Series, Kluwer, Dordrecht, **1991**; b) J. S. Miller, A. J. Epstein, *Angew. Chem.* **1994**, *106*, 399; *Angew. Chem. Int. Ed. Engl.* **1994**, *33*, 385; c) O. Kahn, *Molecular Magnetism*, VCH, New York, **1993**; d) *Molecular Magnetism: from Molecular Assemblies to the Devices* (Eds.: E. Coronado, P. Delhaès, D. Gatteschi, J. S. Miller), NATO ASI Series, Kluwer, Dordrecht, **1996**; e) *Magnetic Properties of Organic Materials* (Ed.: P. M. Lahti), Marcel Dekker, New York, **1999**; f) *Molecular Magnetism: New Magnetic Materials* (Eds.: K. Itoh, M. Kinoshita), Gordon and Breach, Amsterdam, **2000**; g) *π-Electron Magnetism: From Molecules to Magnetic Materials* (Ed.: J. Veciana), Structure and Bonding, vol. 100, Springer, **2001**; h) *Magnetism: Molecules to Materials (I–IV)* (Eds.: J. S. Miller, M. Drillon), Wiley-VCH, Weinheim, **2003**.

[2] a) E. D. Dagotto, T. M. Rice, *Science* **1996**, *271*, 618; b) B. Frischmuth, B. Ammon, M. Troyer, *Phys. Rev. B* **1996**, *54*, R3714; c) M. Greven, R. J. Birgeneau, U.-J. Wiese, *Phys. Rev. Lett.* **1996**, *77*, 1865; d) T. Barnes, E. Dagotto, J. Riera, E. S. Swanson, *Phys. Rev. B* **1993**, *47*, 3196; e) E. Dagotto, J. Riera, D. Scalapino, *Phys. Rev. B* **1992**, *45*, 5744; f) S. R. White, R. M. Noack, D. J. Scalapino, *Phys. Rev. Lett.* **1994**, *73*, 886; g) M. Troyer, H. Tsunetsugu, D. Würtz, *Phys. Rev. B* **1994**, *50*, 13515; h) T. Barnes, J. Riera, *Phys. Rev. B* **1994**, *50*, 6817.

[3] a) C. Galeriu, M. A. Thesis, Dept. of Physics, Clark University, **2002**. Originally, a Heisenberg Hamiltonian such as $H = +\Sigma(J_{AB}{\cdot}S_A{\cdot}S_B)$ was used, and so positive *J* parameters correspond to antiferromagnetic interactions. Thus, in order to be consistent with Heisenberg Hamiltonian (1) we have translated J_{rung} and J_{rail} into –14.16 and –13.59 cm^{-1}, respectively; b) M. M. Turnbull, C. Galeriu, J. Giantsidis, C. P. Landee, *Mol. Cryst. Liq. Cryst.* **2002**, *376*, 469; c) Johnston et al.; the Monte Carlo expression used for fitting $\chi(T)$ data is available online at the archive website arXiv:cond-mat/0001147.

[4] M. Deumal, M. J. Bearpark, J. J. Novoa, M. A. Robb, *J. Phys. Chem. A* **2002**, *106*, 1299.

[5] The currently available magneto-structural correlations for through-space magnetic interactions, the so-called McConnell-I and McConnell-II mechanisms, lack a solid theoretical foundation and fail to properly describe the nature of the magnetic interactions in many crystals. For studies of these failures, see: a) M. Deumal, J. Cirujeda, J. Veciana, J. J. Novoa, *Adv. Mater.* **1998**, *10*, 1461; b) M. Deumal, J. Cirujeda, J. Veciana, J. J. Novoa, *Chem. Eur. J.* **1999**, *5*, 1631; c) M. Deumal, J. J. Novoa, M. J. Bearpark, P. Celani, M. Olivucci, M. A. Robb, *J. Phys. Chem. A* **1998**, *102*, 8404; d) C. Kollmar, O. Kahn, *Acc. Chem. Res.* **1993**, *26*, 259.

[6] In our first papers[4,7a–7c] we used the term "magnetic structure" for this property. In this paper we have re-named it as "magnetic topology" in order to avoid misunderstandings with experimental information related to polarized neutron diffraction measurements.

[7] a) M. Deumal, M. A. Robb, J. J. Novoa, *Polyhedron* **2003**, *22*, 1935; b) M. Deumal, C. P. Landee, J. J. Novoa, M. A. Robb, M. M. Turnbull, *Polyhedron* **2003**, *22*, 2235; c) M. Deumal, J. Ribas-Ariño, M. A. Robb, J. Ribas, J. J. Novoa, *Molecules* **2004**, *9*, 757; d) M. Deumal, M. J. Bearpark, M. A. Robb, Y. Pontillon, J. J. Novoa, *Chem. Eur. J.* **2004**, *10*, 6422.

[8] M. M. Turnbull, C. P. Landee, B. W. Wells, *Coord. Chem. Rev.* **2005**, in press.

[9] The Madelung field was taken into account by selecting all first nearest neighbors surrounding the two $CuBr_4^{2-}$ and four $5NAP^+$ clusters, i.e. 34 radical $CuBr_4^{2-}$ anions and 68 closed shell $5NAP^+$ cations, and attributing to the atoms of such molecules a Merz–Singht–Kollman charge (ref.[10]). The charges used are shown in Table S1.

[10] Electrostatic potential-derived charges according to the Merz–Singht–Kollman scheme: a) B. H. Besler, K. M. Merz Jr., P. A. Kollman, *J. Comput. Chem.* **1990**, *11*, 431; b) U. C. Singh, P. A. Kollman, *J. Comput. Chem.* **1984**, *5*, 129.

[11] The Heisenberg Hamiltonian (1) is used for diagonalization purposes in order to obtain all the energy eigenvalues required in the statistical mechanics expression of $\chi(T)$. For a numerical calculation of the energy eigenvalues, we use *J*(*di*)/2 values (–11.085, –9.865, –0.425, and –0.155 cm^{-1}) rather than *J*(*di*) values (–22.17, –19.73, –0.85, and –0.31 cm^{-1}) in Hamiltonian (1) in order to be consistent with the definition of *J*(*di*).

[12] The 11 K value for the singlet–triplet gap was determined experimentally using the equation: $(E_1 - E_0) = g{\cdot}\mu_B{\cdot}H_{C1}$, where *g* is the gyromagnetic factor ($g = 2.15$, for a polycrystalline sample), μ_B is the Bohr magneton, and H_{C1} is the critical field. The lower critical field was determined to be 7.6 T from the magnetization data collected at 0.65 K.

[13] a) L. Noodlemann, *J. Chem. Phys.* **1981**, *74*, 5737; b) L. Noodlemann, E. R. Davidson, *Chem. Phys.* **1986**, *109*, 131.
[14] a) E. Ruiz, P. Alemany, S. Alvarez, J. Cano, *J. Am. Chem. Soc.* **1997**, *119*, 1297; b) R. Caballol, O. Castell, F. Illas, I. D. R. Moreira, J. P. Malrieu, *J. Chem. Phys. A* **1997**, *101*, 7860; c) M. Nishino, Y. Shigeta, T. Soda, Y. Kitagawa, T. Onishi, Y. Yoshioka, K. Yamaguchi, *Coord. Chem. Rev.* **2000**, *198*, 265; d) J.-M. Mouesca, *J. Chem. Phys.* **2000**, *113*, 10505; e) F. Illas, I. D. R. Moreira, C. de Graaf, V. Barone, *Theor. Chem. Acc.* **2000**, *104*, 265.
[15] a) A. D. Becke, *Phys. Rev. A* **1988**, *38*, 3098; b) C. Lee, W. Yang, R. G. Parr, *Phys. Rev. B* **1988**, *37*, 785; c) A. D. Becke, *J. Chem. Phys.* **1993**, *98*, 5648.
[16] M. J. Frisch, G. W. Trucks, H. B. Schlegel, G. E. Scuseria, M. A. Robb, J. R. Cheeseman, J. A. Montgomery Jr., T. Vreven, K. N. Kudin, J. C. Burant, J. M. Millam, S. S. Iyengar, J. Tomasi, V. Barone, B. Mennucci, M. Cossi, G. Scalmani, N. Rega, G. A. Petersson, H. Nakatsuji, M. Hada, M. Ehara, K. Toyota, R. Fukuda, J. Hasegawa, M. Ishida, T. Nakajima, Y. Honda, O. Kitao, H. Nakai, M. Klene, X. Li, J. E. Knox, H. P. Hratchian, J. B. Cross, C. Adamo, J. Jaramillo, R. Gomperts, R. E. Stratmann, O. Yazyev, A. J. Austin, R. Cammi, C. Pomelli, J. W. Ochterski, P. Y. Ayala, K. Morokuma, G. A. Voth, P. Salvador, J. J. Dannenberg, V. G. Zakrzewski, S. Dapprich, A. D. Daniels, M. C. Strain, O. Farkas, D. K. Malick, A. D. Rabuck, K. Raghavachari, J. B. Foresman, J. V. Ortiz, Q. Cui, A. G. Baboul, S. Clifford, J. Cioslowski, B. B. Stefanov, G. Liu, A. Liashenko, P. Piskorz, I. Komaromi, R. L. Martin, D. J. Fox, T. Keith, M. A. Al-Laham, C. Y. Peng, A. Nanayakkara, M. Challacombe, P. M. W. Gill, B. Johnson, W. Chen, M. W. Wong, C. Gonzalez, J. A. Pople, *Gaussian 03*, Revision B.04, Gaussian, Inc., Pittsburgh, PA, **2003**.
[17] Ahlrichs' pVDZ basis set: A. Schafer, H. Horn, R. Ahlrichs, *J. Chem. Phys.* **1992**, *97*, 2571.
[18] 6-31+G split-valence basis set: a) P. C. Hariharan, J. A. Pople, *Theor. Chim. Acta* **1973**, *28*, 213; b) M. M. Francl, W. J. Petro, W. J. Hehre, J. S. Binkley, M. S. Gordon, D. J. DeFrees, J. A. Pople, *J. Chem. Phys.* **1982**, *77*, 3654.
[19] 6-31+G(d) basis set: a) R. C. Binning Jr., L. A. Curtiss, *J. Comput. Chem.* **1990**, *11*, 1206; b) Primitive Exponents: T. H. Dunning Jr., *J. Chem. Phys.* **1977**, *66*, 1382.

Received: May 31, 2005
Published Online: October 25, 2005

